The Role of Roles: Physical Cooperation between Humans and Robots

Alexander Mörtl, Martin Lawitzky, Ayse Kucukyilmaz,
Metin Sezgin, Cagatay Basdogan and Sandra Hirche

Draft: March 15, 2012

Abstract

Since strict separation of working spaces of humans and robots experiences a softening due to recent robotics research achievements, close interaction of humans and robots comes rapidly into reach. In this context, physical human-robot interaction raises a number of questions regarding a desired intuitive robot behavior. The continuous bilateral information and energy exchange requires an appropriate continuous robot feedback. Investigating a cooperative manipulation task, the desired behavior is a combination of an urge to fulfill the task, a smooth instant reactive behavior to human force inputs and an assignment of the task effort to the cooperating agents. In this paper, a formal analysis of human-robot cooperative load transport is presented. Three different possibilities for the assignment of task effort are proposed. Two proposed dynamic role exchange mechanisms adjust the robot's urge to complete the task based on the human feedback. For comparison, a static role allocation strategy not relying on the human agreement feedback is proposed as well. All three role allocation mechanisms are evaluated in a user study that involves large-scale kinesthetic interaction and full-body human motion. Results show tradeoffs between subjective and objective performance measures stating a clear objective advantage of the proposed dynamic role allocation scheme.

1 Introduction

A variety of physical tasks require the cooperation of two or more agents and demands for haptic joint action of multiple partners, robots together with humans. In such kind of tasks, humans interact and communicate in different modalities: *verbally* e.g. through speech and also *non-verbally* e.g. through gestures and the sense of touch. The twofold feature of haptic interaction is particularly challenging: Physical coupling allows the agents to negotiate and accomplish the joint action task simultaneously. This means that intuitive interaction is mediated by task oriented actions. Additionally, the strong implicit nature of the haptic communication channel requires sophisticated interpretive capabilities to understand the partners' behavior on a fast time scale. One keypoint to be negotiated is the necessary effort to accomplish cooperative physical tasks which must be continuously allocated among all contributors. Observable effects of negotiation are emerging strategies in terms of temporally consistent haptic interaction patterns called *specialization* (Reed et al., 2006). In physical cooperation, these patterns refer to a self-organized distribution of the agents' individual contributions. Forming patterns of interaction seems to ease mutual understanding of partners, as improved task performance has been observed repeatedly in cooperative settings (Feth et al., 2009; Reed et al., 2005). As soon as autonomous physical assistants are able to produce their own task-directed behavior, the question of role assignment arises similarly. Observations from human-human cooperation or motion

planning techniques can be used by the robot to calculate its own necessary force contribution to achieve task progress. However, the assignment and possible re-allocation of roles can evolve during task execution and cannot be pre-computed. The resulting challenge is the synthesis of a robotic assistant that takes the human habit to establish and dynamically change roles into account and renders an intuitive behavior to the human partner. Therefore an understanding of the physical meaning of roles in human-robot cooperative manipulation helps to develop a framework for role allocation.

Some work on the derivation of guidelines for the synthesis of a robotic role allocation from observations of human-human behavior exists. However, related existing approaches towards autonomous physical robotic helpers target mainly the smooth and intuitive reactive behavior of robots in physical interaction with humans rather than situation-dependent active task contribution. Only little related research on the topic of role adaptation in physical human-robot interaction exists.

Oguz et al. (2010) proposed a haptic negotiation framework for blending between dominant and recessive control states in a dynamic virtual task. Their system realizes dynamic role exchange by granting control to one of the operators regarding the intentions of the human, who was assumed to display the intention of gaining control by applying large forces to the system. Later, Kucukyilmaz et al. (2011) showed that this dynamic role exchange scheme improved task efficiency significantly when compared to an equal control guidance scheme and constituted a personal and subjectively pleasing interaction model.

In a similar scenario, Passenberg et al. (2011) introduced adaptable haptic assistance in a shared control setup. They used human effort and task performance criteria to find static optimal assistance levels for certain tasks and outlined possibilities for implementing on-line adaptation. Abbink et al. (2012) provide a comprehensive review on haptic shared control accompanied by design guidelines to be considered for such interactive systems. Despite many inspiring affinities between haptic shared control and human-robot physical role allocation, differences emerge from human interaction with a physical entity: In shared control scenarios, approaches rely on the possibility to adjust either the coupling between the human operator and the virtual object, or the coupling between the operator and the virtual assistant both acting on the same control interface. In scenarios involving physical robotic assistants, the missing option to control the human partner's coupling with the object as well as the varying coupling of partners through the object impose additional challenges.

The main contribution of this work is a set of strategies for static and dynamic role allocation in haptic human-robot cooperation and an experimental evaluation of the proposed strategies. The task of cooperative human-robot object manipulation is analyzed in redundant and non-redundant degrees of freedom. The meaning of effort sharing along the redundant degrees of freedom is derived. A user study shows the effects of three different effort sharing strategies on task performance and subjective acceptance in a realistic large-scale scenario.

1.1 Related Work

The synthesis of physical robotic assistants for cooperative load sharing tasks reaches back to the early 1990's when Kosuge et al. (1993) deployed an object-centered impedance control scheme similar to Schneider and Cannon (1992) for a set of robots cooperating with a number of humans.

Successful hardware implementations named *MR Helper* and the distributed variant *DR Helpers* (Hirata and Kosuge, 2000) encouraged a number of groups to research synthesis methods for cooperative human-robot object manipulation strategies. An overview of the achievements of Hirata and Kosuge in this field is given in Kosuge and Hirata (2004). The application of cooperative load transport has also been targeted by Gillespie et al. (2001) using the rather different *Cobot* approach. While Kosuge's robotic helpers could actively render a virtual object impedance behavior with features such as collision avoidance, *Cobots* cannot move on their own – they are inherently passive. However, motion induced by a human operator is projected along virtual curvatures by arranging counter-acting forces in the *Cobots*. This approach focuses on desired paths or

workspace constraints rather than desired virtual dynamic object behavior, similar to the *virtual fixtures* introduced by Rosenberg (1993) as overlays such as virtual rulers guiding the operator's effector motion in telepresence setups. An approach combining desired virtual constraints and desired virtual object dynamics was proposed by Takubo et al. (2002). In their work, a robotic partner renders a virtual nonholonomic constraint – namely a virtual wheel – that prohibits sideway slipping motion and thus simplifies operation similar to a wheelbarrow. This simplification however, inhibits maneuvering of bulky objects in narrow passages. The group of Ikeura investigated the feedback behavior of a following manipulator during cooperative object transport. Human impedance characteristics were found to be the best in terms of subjective scores (Ikeura et al., 1994) and to enable natural movement profiles (Ikeura et al., 2002). All of these approaches consider robotic partners that react on user operation which certainly limits these devices' capabilities.

In order to overcome such limitations, a significant body of work was dedicated to fundamentally model human behavior in cooperative haptic tasks and to transfer findings to cooperative robotic partners. The popular concept of jerk minimization in human arm movements as proposed by Flash and Hogan (1985) for pointing has been transferred to cooperative manipulation by Maeda et al. (2001). This enabled a robotic partner to not just react to a human operator input but also to predict human intentions and act accordingly. Reed et al. (2005, 2006) investigated the effects of specialization in human-human interaction and successfully transferred their results to a human-robot setup so well that participants could not distinguish between the robotic partner and an actual human partner (Reed and Peshkin, 2008). Reed's findings on evolving specialization were further investigated by Groten et al. (2009) who showed that users prefer a dominance difference among collaborating partners in contrast to equally shared control. In this context, dominance refers to the actual achievement of influence or control over another and therefore reflects the individual share of the overall contribution to task success.

In order to decide on the necessary overall contribution, first, the desired trajectory must be known. Miossec and Kheddar (2008) discovered a motion model for cooperating humans that outperforms the minimum-jerk model used by Maeda et al. (2001). Based on this trajectory generation method for cooperative object moving tasks, Evrard and Kheddar (2009) developed a controller blending scheme that allow a leader/follower role allocation with one single blending parameter. Recent insights on leader/follower assignment from this group can be found in (Kheddar, 2011) which suggests that blending of stable leader and follower controllers will not necessarily result in a stable overall behavior. Human following behavior as a response to a leading robotic manipulator has been investigated in a cooperative vertical lifting task by Parker and Croft (2011). Behavioral hallmarks such as different frequency domains of human visual and haptic response could be discovered. An overall system architecture that comprises a confidence-based role adaptation, implemented on a very small scale humanoid robot was recently presented by Thobbi et al. (2011).

An emerging interest in smart physical robotic assistants for human workers in industrial settings is visible for a few years. Wojtara et al. (2009) developed a basic physical assistant for the well defined task of precise positioning of windshields during car manufacturing processes. Their framework proposes a strict geometrical separation of the degrees of freedom and weighs the assistant's force contribution to the task according to haptic cues.

1.2 Contribution

The main contribution of this work is an investigation of the objective and subjective effects of dynamic role allocation for a physical robotic assistant. Therefore, the task of cooperative load transport is analyzed and decomposed into two components for steering and progressing. Meaningful decomposition parameterizations are derived such that the necessary effort resulting from a desired task progress is allocated among the cooperating partners. Therefore we propose three different strategies: First, a constant role allocation disregarding the human's haptic expression of the desire to accelerate or decelerate the

task progress. Secondly, a continuous adjustment of the allocated roles depending on human feedback and thirdly, a discretized version of the second approach. Within a user study involving large-scale kinesthetic interaction in a realistic scenario with human full body motion, the proposed approaches are evaluated in terms of task performance and user acceptance.

1.3 Notation

In this article, bold characters are used for denoting vectors and matrices. $\mathrm{Ker}(\boldsymbol{A})$ denotes the kernel or nullspace of matrix $\boldsymbol{A}$. $\mathrm{Ker}_j(\boldsymbol{A})$ denotes the j^{th} vector spanning $\boldsymbol{A}$'s nullspace. A matrix's *nullity* is the dimension of its nullspace. Superscripts are used to denote the reference frame of the respective matrix and vector quantities, whereas quantities referring to the inertial frame are written without superscripts.

The remainder of this article is structured as follows: The problem is stated and confined in Section 2 where also our conceptual approach is presented. Section 3 gives a systematic analysis of the envisaged task and explains the meaning of roles. The deployed control scheme is presented in Section 4. Our experimental setup is depicted in Section 5. The evaluation methods used are explained in Section 6 and the results are presented in Section 7. A discussion of the results is given in Section 8 and we conclude and give an outlook in Section 9.

2 Problem definition and approach

Our work addresses the cooperative task of jointly manipulating a rigid bulky object by human-robot teams. In the following, we concisely define our problem and outline our conceptual approach.

2.1 Definition of the effort sharing problem

The envisaged scenario allows the *cooperation* between a human and an assistive robot. Parker (2008) and Olfati-Saber et al. (2007) define cooperation as

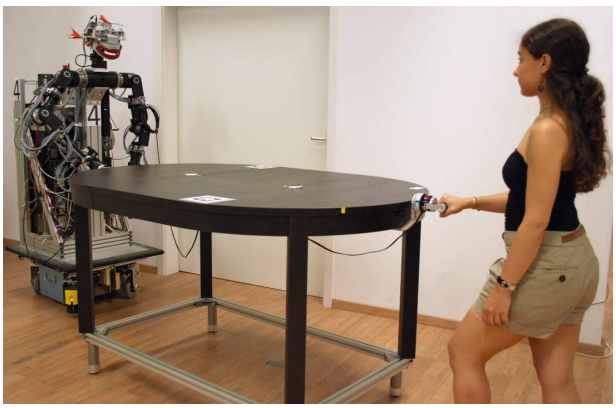

Figure 1: The cooperative manipulation scenario and the experimental setup: human and robot jointly transporting a bulky table.

the willing participation of all agents towards a common goal along a shared plan. In line with this, we focus on manipulation tasks which require physical cooperation between partners through close coupling with an object, see Fig. 1. When two or more agents cooperate through jointly manipulating a common object, the problem of sharing the task's physical effort arises. The physical coupling imposed by the task's geometrical and dynamical properties has to be addressed and exploited such that each agent's effort in terms of input wrenches allow for a smooth and efficient cooperation. We confine the effort sharing problem to the following conditions:

- One human *cooperates* with one robot / system of robots with centralized communication towards achieving a common known goal (e.g. reaching certain configuration(s) when jointly manipulating an object).
- Constraints of the environment are such that the task is achievable (e.g. a feasible path to the goal exists).
- All participants *tightly grasp* a single *rigid* object with commonly known shape and dynamics.
- Object dynamics are holonomic, i.e. the manipulated system does not have any velocity-dependent constraints.

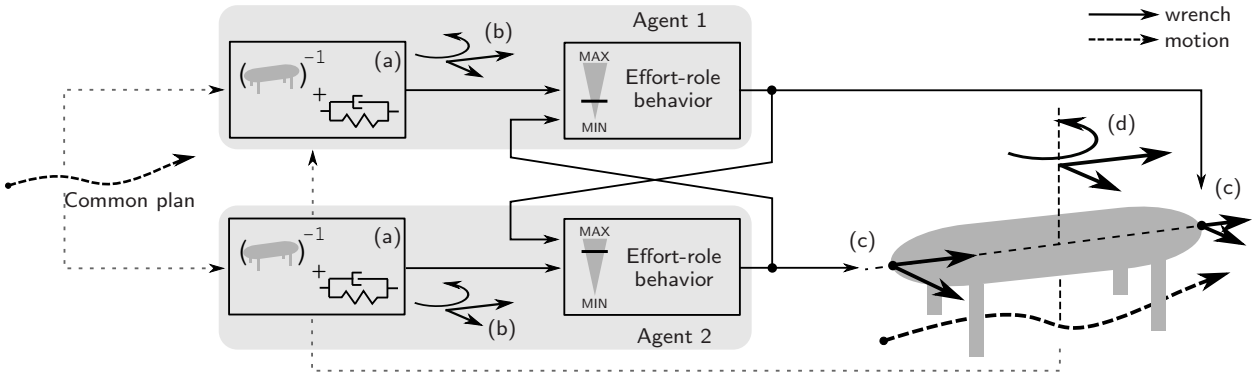

Figure 2: Overview of the modeling approach: A dyad consisting of agent 1 and agent 2 cooperatively manipulates a common object according to a shared plan. Both agents employ an inverse object model and impedance control loop (a) generating desired object-centered wrenches (b). The effort-role behavior determines the control inputs applied at the agents' grasp points (c) which compose the object-centered wrench (d) required for motion tracking. Roles are allocated by mutual feedback of the control inputs.

- The grasp points are such that the task is *controllable* and its control inputs are *redundant* (Lawitzky et al., 2010).
- The partners interact with each other only through the haptic channel provided by the physical coupling.

2.2 System-theoretic modeling approach

A dynamic modeling approach of the task is employed to define the physical and geometrical properties of the manipulation task under environmental constraints. Through this approach, we model the dynamics of the manipulated object including the agents' contact points, see Fig. 2. Starting from an object-centered viewpoint, the agents' contributions to the task can be defined by spatially distributed control inputs, i.e. forces that affect the object's motion towards the goal.

Results on the cooperation of human dyads suggest an object-centered formulation of the desired path, as they achieve better tracking performance in a cooperative task when they have common visual access to the central part of a manipulated object (Salleh et al., 2011). Thus, the desired motion of the manipulated object can be intuitively represented by an object-centered trajectory as a result of a priori negotiation between the agents. Impedance control loops closed on motion feedback and employed by each agent ensure tracking of the desired object trajectory. In this article, we assume shared goals in terms of known intermediate configurations of the manipulated object. A path for the cooperating dyad can be precomputed by the robot from planning as proposed by Kirsch et al. (2010) or from human demonstration (Medina et al., 2011).

Furthermore, the object model is assumed to be known to all agents, and in order to obtain the required individual control inputs for motion tracking, each agent applies an inverse dynamics model of the object. While the human motor control system is known to accomplish haptic tasks by a combination of impedance control and inverse dynamics model of the task (see e.g. Franklin et al., 2003), automatic parameter acquisition for rigid body loads is a difficult problem, which has been frequently discussed in the literature since Atkeson et al. (1986). Also state-of-the-art methods require structural knowledge of the friction phenomena involved. Therefore, we address the manipulation of objects known to the robot in terms of their geometry, grasp points and relevant

dynamical properties.

This is where the demand for an *effort sharing strategy* comes into play: redundancies of the control inputs, which are usually present if two or more agents are manipulating a single object (Lawitzky et al., 2010), span a subspace of the control inputs which can be deliberately distributed between the agents without affecting the motion.

Effort sharing describes the distribution of voluntary force inputs among agents. Each agent can be assigned a certain input behavior in terms of an effort sharing policy. The behavioral patterns of the agents due to a certain effort sharing policy can be referred to as *roles* that the agents take on in the redundant task space. The effort-role behavior synthesized in this paper is embedded in the interaction control loop and mediates the robotic agent's control inputs to the task.

While a feedforward assignment of roles in a centralized manner works well for robotic agents, such an assignment is inappropriate for humans. Investigation of human cooperative behavior in a dyadic tracking task provides evidence for role distributions, which are partly person-specific and partly interaction-dependent (Groten et al., 2009). If we assume persistent validity of the agents' shared plan which holds true for a static environment, the applied input of a *single human agent* can be estimated based on the object dynamics and fed back to allocate the agents' roles on-line. Assuming a manipulation system which allows for measurements of the human input forces, *multiple human agents* may be considered to contribute to the task. In this article, we develop concepts for role allocation within a human-robot dyad and evaluate these concepts with an experimental study.

3 Synthesis of role behavior

This section presents the object model and a parameterization method for effort sharing policies. Different sharing policies and the definition of roles we adopt in the experiments are explained. Our method to parameterize effort sharing policies generalizes to multiple cooperating partners. Therefore in the first part of the derivations we will keep the method as general as possible and later specialize to the dyadic case.

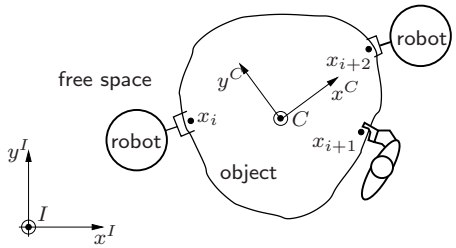

Figure 3: Haptic human-robot joint action task: Cooperative manipulation of a rigid object by multiple agents acting at different grasp points.

3.1 Object model

The general problem of joint transfer of an object in free space involves the contribution of N agents that tightly grasp a rigid object of arbitrary shape as shown in Fig. 3. In the figure, a body frame C is attached to the object and the inertial frame is denoted by I. Besides a collision-free trajectory in compliance with the environment, the dynamical and geometrical model of the manipulated object – the coupling between the agents – is crucial to a system-theoretic analysis of the task.

We assume that the rigid-body dynamics of the object can be described by

$$\boldsymbol{M}_c\ddot{\boldsymbol{x}}_c + \boldsymbol{f}_c(\boldsymbol{x}_c, \dot{\boldsymbol{x}}_c) = \boldsymbol{u}_c, \tag{1}$$

where $\boldsymbol{x}_c$ is the configuration of the object with inertia $\boldsymbol{M}_c$, $\boldsymbol{f}_c$ is the sum of environmental forces such as friction and gravitation, and $\boldsymbol{u}_c$ denotes the *external wrench* applied by the agents to the object.

Agent i contributes to the manipulation task via input wrench $\boldsymbol{u}_i$ applied at the grasp point $\boldsymbol{x}_i$ on the object, $i = 1, ..., N$. In order to formally represent the type of grasp and to consider only the efficient input wrench components of the agents, we introduce the *applied wrench* $\tilde{\boldsymbol{u}}_i$ as

$$\tilde{\boldsymbol{u}}_i = \boldsymbol{R}\boldsymbol{B}_i\boldsymbol{R}^T\boldsymbol{u}_i, \tag{2}$$

where $\boldsymbol{R}$ denotes the rotation of frame C w.r.t. I and $\boldsymbol{B}_i$ is a selection matrix referred to the body frame C with elements $b_{k,l} = \{0, 1\}$ determining which independent torque and force components an agent can effectively apply at the grasp point. Note that $\boldsymbol{B}_i$ is also known as wrench basis in grasp analysis (Murray et al., 1994). Thus, the external wrench on the object is composed by

$$\boldsymbol{u}_c = \sum_{i=1}^{N} \boldsymbol{G}_i \tilde{\boldsymbol{u}}_i, \tag{3}$$

where matrix $\boldsymbol{G}_i$ ($\dim(\tilde{\boldsymbol{u}}_i) \times \dim(\boldsymbol{u}_c)$) denotes the partial grasp matrix (Prattichizzo and Trinkle, 2008). It is given by the Jacobian of the kinematic constraints $\boldsymbol{\phi}_i(\boldsymbol{x}_c)$ which describes the position of the rigid grasp point with respect to the object frame. The kinematics comprising position $\boldsymbol{x}_i$ and velocity $\dot{\boldsymbol{x}}_i$ of the grasp point of agent i are

$$\boldsymbol{x}_i = \boldsymbol{\phi}_i(\boldsymbol{x}_c) \tag{4}$$
$$\dot{\boldsymbol{x}}_i = \boldsymbol{G}_i^T \dot{\boldsymbol{x}}_c. \tag{5}$$

In the following, the dynamics and kinematics of the object grasped by the agents serve as a basis for analysis of the effort sharing problem.

3.2 Effort sharing by input decomposition

In this section, we develop a strategy for effort sharing which utilizes *redundant* degrees of freedom that naturally arise from actuation redundancy. According to our system-theoretic approach outlined in Section 2.2, with the inverse dynamical system model (1) a desired external wrench $\hat{\boldsymbol{u}}_c$ can be calculated, which is to be imposed on the object to track a shared plan given as a desired trajectory of the object configuration $\boldsymbol{x}_{c,d}$. Note that in general, only parts of the applied wrenches cause the object's motion and hence constitute the external wrench. The remaining component of the applied wrench is called *internal wrench* and causes squeeze forces on the object. In the next step, we aim for solutions of each agent's applied wrench $\tilde{\boldsymbol{u}}_i$, in order to compose a desired $\hat{\boldsymbol{u}}_c$.

By substituting (3) into (1), we obtain for the object model

$$\boldsymbol{M}_c \ddot{\boldsymbol{x}}_c + \boldsymbol{f}_c(\boldsymbol{x}_c, \dot{\boldsymbol{x}}_c) = \boldsymbol{G}\tilde{\boldsymbol{u}}, \tag{6}$$

with the complete grasp matrix $\boldsymbol{G}$ composed by the block diagonal matrix

$$\boldsymbol{G} = \operatorname{diag}\left\{ \begin{array}{cccc} \boldsymbol{G}_1, & \ldots, & \boldsymbol{G}_N \end{array} \right\},$$

and the stacked applied wrench

$$\tilde{\boldsymbol{u}} = \left[\begin{array}{ccc} \tilde{\boldsymbol{u}}_1 & \ldots & \tilde{\boldsymbol{u}}_N \end{array} \right]^T.$$

Let us introduce now

$$\tilde{\boldsymbol{u}} = \boldsymbol{A}\hat{\boldsymbol{u}}_c, \tag{7}$$

where $\boldsymbol{A}$ denotes a decomposition matrix from desired external wrenches to applied wrenches. Using (7), the dynamical object model depending on the desired external wrench yields

$$\boldsymbol{M}_c \ddot{\boldsymbol{x}}_c + \boldsymbol{f}_c(\dot{\boldsymbol{x}}_c) = \boldsymbol{G}\boldsymbol{A}\hat{\boldsymbol{u}}_c.$$

In order to achieve tracking of the desired trajectory through feedforward control of the inverse dynamics, matrix $\boldsymbol{A}$ has to be chosen to sustain $\boldsymbol{u}_c = \hat{\boldsymbol{u}}_c$, i.e. $\boldsymbol{A}$ has to be an inverse of $\boldsymbol{G}$, fulfilling

$$\boldsymbol{G}\boldsymbol{A} = \boldsymbol{I}. \tag{8}$$

Note that $\dim(\boldsymbol{u_c})$ is equal to the dimension of the object's configuration space $\dim(\boldsymbol{x}_c)$, since the task is required to be controllable and holonomic. In our setting, we further assume that the number of actual inputs is larger than the required number of inputs for task completion,

$$\dim(\tilde{\boldsymbol{u}}) > \dim(\boldsymbol{u}_c).$$

A minimal example of such actuation redundancy is the movement of an object in one-dimensional space by two agents, each applying an input wrench. The task is redundant as one agent's input would be sufficient for controlling the object, and arbitrary compositions of the agent's input forces are possible, see Fig. 4. Therefore, the choice of $\boldsymbol{A}$ in (8) is not unique.

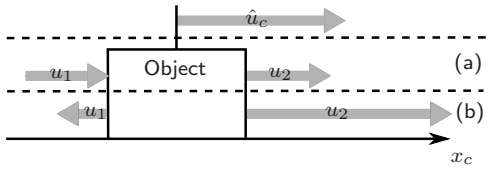

Figure 4: Illustrative example of input decomposition in a one-dimensional redundant task. (a) minimum-norm solution. (b) possible, but inefficient solution.

We can show that a particularly interesting solution for the effort-sharing matrix $\boldsymbol{A}$ is the generalized *Moore-Penrose* pseudoinverse $\boldsymbol{G}^+$ of the complete grasp matrix $\boldsymbol{G}$, which yields the minimum-norm solution for $\|\tilde{\boldsymbol{u}}\|$ (Doty et al., 1993). Since we are solving for wrenches, there is particular physical meaning of the minimum-norm solution: The applied wrench obtained with $\boldsymbol{G}^+$ represents an *efficient* decomposition, because the external wrench is composed by a minimum magnitude of the applied wrench's components, see Fig. 4 (a). Hence, the applied wrench has no components which could cause ineffective internal wrenches.

Additionally, the nullspace of $\boldsymbol{G}$ defined as

$$\mathrm{Ker}(\boldsymbol{G}) = \{\tilde{\boldsymbol{u}} | \boldsymbol{G}\tilde{\boldsymbol{u}} = \boldsymbol{0}\}$$

provides a solution space for $\tilde{\boldsymbol{u}}$. Note that in a physical meaning, the null-space component causes no motion of the object, as it does not affect the external wrench. When we replace $\boldsymbol{A}$ by $\boldsymbol{G}^+$ in (7), the family of all solutions for $\tilde{\boldsymbol{u}}$ is given by

$$\tilde{\boldsymbol{u}} = \boldsymbol{G}^+ \hat{\boldsymbol{u}}_{\boldsymbol{c}} + \sum_{j=1}^{\mathrm{nullity}(\boldsymbol{G})} \lambda_j \mathrm{Ker}_j(\boldsymbol{G}), \qquad (9)$$

with parameter $\lambda_j \in \mathbb{R}$. Depending on the choice of λ_j, the solution $\tilde{\boldsymbol{u}}$ potentially produces internal wrenches, as depicted in Fig. 4 (b). In fact, solution (9) provides an effort sharing strategy by input decomposition: In *redundant* degrees of freedom where effort sharing between the agents can take place and which are affected by λ_j, and in *non-redundant* degrees of freedom where each agent's input is uniquely defined by a necessary contribution.

In the following section we show how λ_j can be used to parameterize the effort sharing strategy between the agents in a single redundant direction.

3.3 Policies for effort sharing

In this section we show how the agents can be assigned meaningful policies regarding their effort behavior in a single redundant degree of freedom. With reference to the experiment conducted in this study and for intuitiveness of analysis, we consider from this section on a planar cooperative manipulation task involving two agents for the design of effort sharing policies without loss of generality. The presented strategy may be conducted in multiple redundant degrees of freedom.

3.3.1 Analysis of a planar dyadic task

An example planar dyadic task is shown in Fig. 5, which satisfies the requirements from Section 2.1. The joint transport of a large table on ball casters,

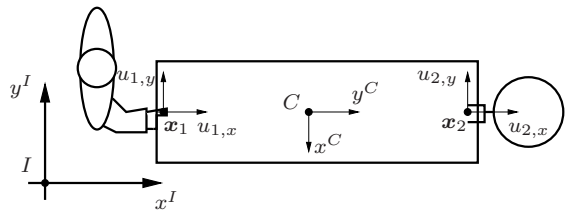

Figure 5: Illustrative scenario of planar cooperative manipulation: one human (left) and one robot (right) jointly move a bulky object in the x-y-plane.

or the joint movement of any other heavy object by sliding it on a surface can be such a task. Both, the human (i=1) and the robotic agent (i=2) could provide input wrenches $\boldsymbol{u}_i$ of dimension $\dim(\boldsymbol{x}_c)$ with

$$\boldsymbol{x}_c = \begin{bmatrix} x_{c,\phi} & x_{c,x} & x_{c,y} \end{bmatrix}^T,$$

which generally include torques. However, a common property of bulky objects regarding their handling is the lack of sensitivity of object dynamics to certain torque components, meaning that these torques cannot be applied effectively at the grasp points (see also

Wojtara et al., 2009). This can be explained within our illustrative scenario. Assume a beam-like bulky object with a long geometrical axis, which is manipulated by two partners using a single-handed grasp on the respective end of the object, see Fig. 5. In order to induce a desired rotational motion around the z^C-axis, from experience the reader might agree that it is rather cumbersome to apply the required torque component through the wrist. It is much easier to apply an appropriate force component through the whole arm which induces turning by translational motion of the grasp point.

Since our analysis focuses on the primary effects of the system's redundant degrees of freedom for effort sharing, the wrench basis

$$\boldsymbol{B}_{1,2} = \begin{bmatrix} 0 & 1 & 0 \\ 0 & 0 & 1 \end{bmatrix}$$

is chosen in our illustrative scenario. Putting it into (2) reduces the input wrench to the effectively applied wrench

$$\tilde{\boldsymbol{u}} = \begin{bmatrix} u_{1,x} & u_{1,y} & u_{2,x} & u_{2,y} \end{bmatrix}^T. \tag{10}$$

The kinematic constraints (4) of the system can be written as

$$\boldsymbol{x}_i = \begin{bmatrix} x_{c,x} & x_{c,y} \end{bmatrix}^T - \boldsymbol{R}\boldsymbol{r}_{ic}^C,$$

with

$$\boldsymbol{R} = \begin{bmatrix} \cos\phi & -\sin\phi \\ \sin\phi & \cos\phi \end{bmatrix}$$

denoting the rotation of object frame C w.r.t. inertial frame I by angle ϕ, and

$$\boldsymbol{r}_{ic}^C = \begin{bmatrix} r_{ic,x} & r_{ic,y} \end{bmatrix}^T$$

being the vectors from the grasp point of agent i to the origin of C. According to (5), the 4×3 transpose of the grasp matrix

$$\boldsymbol{G}^T = \begin{bmatrix} \sin\phi\, r_{1c,x} + \cos\phi\, r_{1c,y} & 1 & 0 \\ -\cos\phi\, r_{1c,x} + \sin\phi\, r_{1c,y} & 0 & 1 \\ \sin\phi\, r_{2c,x} + \cos\phi\, r_{2c,y} & 1 & 0 \\ -\cos\phi\, r_{2c,x} + \sin\phi\, r_{2c,y} & 0 & 1 \end{bmatrix} \tag{11}$$

can be derived. Since we can calculate

$$\forall\phi \quad \dim(\boldsymbol{x}_c) = \operatorname{rank}(\boldsymbol{G}) = 3$$

for different grasp constraints $\boldsymbol{r}_{1,c} \neq \boldsymbol{r}_{2,c} \neq \boldsymbol{0}$, our planar system is redundant regarding the applied wrench (10) since $\dim(\tilde{\boldsymbol{u}}) = 4$.

Thus, parts of the task effort in terms of applied wrenches can be shared arbitrarily among the contributing agents within the redundant degree of freedom without influence on the external wrench of the object. In the following, we introduce *effort sharing policies* which are described by a certain choice of the parameter λ in (9) characterizing meaningful shares. In a first step, we will investigate static sharing policies yielding constant role behaviors, while in Section 3.4 our notion of roles is extended to encompass a dynamic allocation within dyads.

3.3.2 Identification of meaningful policies

In the given planar example, the only redundant degree of freedom is intuitively represented by the y^C-axis of the object frame C (c.f. Fig. 5), hence components of the external input wrench along this axis can be arbitrarily shared among the two agents. Let us recall now decomposition (9) leading to the agents' applied wrenches $\tilde{\boldsymbol{u}}$. The nullspace $\operatorname{Ker}(\boldsymbol{G})$ is spanned by the family

$$\begin{aligned} \operatorname{Ker}(\boldsymbol{G}) &= \operatorname{diag}(\boldsymbol{R}, \boldsymbol{R})\ \operatorname{Ker}(\boldsymbol{G})^C, \text{with} \\ \operatorname{Ker}(\boldsymbol{G})^C &= \begin{bmatrix} 0 & 1 & 0 & -1 \end{bmatrix}^T, \end{aligned} \tag{12}$$

allowing one degree of freedom for the design of different effort sharing policies through the choice of the scalar parameter λ in (9). Three extreme policies of particular physical meaning are discussed below:

- *Balanced-effort policy:* By choosing the policy

  $$\pi_{bal} : \lambda = 0, \tag{13}$$

  we obtain the min-norm solution for $\tilde{\boldsymbol{u}}$. The effort in terms of magnitude of the applied wrench is to be equally shared among the agents, see Fig. 6(a).

- *Maximum-robot-effort policy:* If we want to have the robot to take over all of the sharable effort, then the applied human force in the y^C-direction would be zero, i.e. $\tilde{u}_{1,y}^C = 0$. Hence, λ is chosen

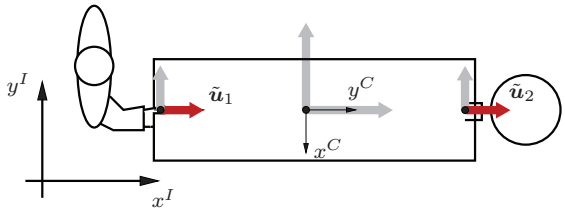

(a) Equal share of the voluntary effort.

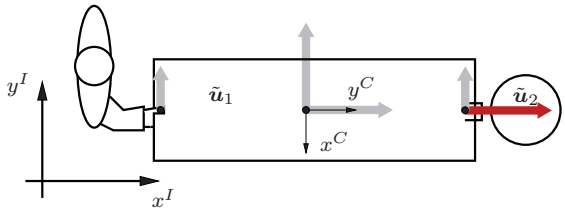

(b) Robot takes all of the voluntary effort.

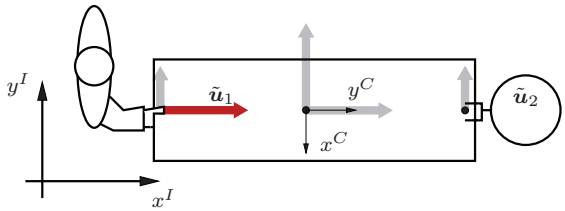

(c) Human takes all of the voluntary effort.

Figure 6: Given exemplary external wrench realized by three different effort policies.

such that the human does not contribute any *voluntary* effort to the task, which yields the policy

$$\pi_{max} : \lambda = -\begin{bmatrix} 0 & 1 & 0 & 0 \end{bmatrix} \tilde{\boldsymbol{u}}^C_{bal}, \tag{14}$$

with the min-norm applied wrench

$$\tilde{\boldsymbol{u}}^C_{bal} = \operatorname{diag}(\boldsymbol{R}, \boldsymbol{R})^T \boldsymbol{G}^+ \hat{\boldsymbol{u}}_{\boldsymbol{c}}. \tag{15}$$

The required human effort in terms of the Euclidean norm

$$\|\tilde{\boldsymbol{u}}^C_1\| = \sqrt{(\tilde{u}^C_{1,x})^2 + (\tilde{u}^C_{1,y})^2}$$

is minimized now, since $\tilde{u}^C_{1,x}$ refers to the necessary input contribution, see Fig. 6(b). Intuitively spoken, the human has to apply wrenches only in those degrees of freedom, which simply *can not* be accomplished by the robot alone, i.e. rotation, and motion in x^C-direction.

- *Minimum-robot-effort policy:* Dual to policy π_{max}, the human has to take over all of the sharable effort, if we satisfy $\tilde{u}^C_{2,y} = 0$ through the policy

$$\pi_{min} : \lambda = \begin{bmatrix} 0 & 1 & 0 & 0 \end{bmatrix} \tilde{\boldsymbol{u}}^C_{bal}, \tag{16}$$

  where $\tilde{\boldsymbol{u}}^C$ is given by (15). Using this policy results in a minimum-effort robot assistance, i.e. in each degree of freedom, the human has to apply wrench components to accomplish the task, see Fig. 6(c).

When we introduce the family of effort sharing policies

$$\pi : \lambda = -\alpha \begin{bmatrix} 0 & 1 & 0 & 0 \end{bmatrix} \tilde{\boldsymbol{u}}^C_{bal}, \tag{17}$$

with *policy parameter* $\alpha \in \mathbb{R}$, obviously the policies π_{bal}, π_{max} and π_{min} are parameterized by setting $\alpha = 0$, $\alpha = 1$ and $\alpha = -1$ respectively.

Note: Policies (17) with $\alpha \in [-1; 1]$ and the kernel family parameterized by (12) are efficient, since no counter-acting internal wrench on the object is generated. Fig. 6(b)–(c) depict the extreme, yet still efficient cases for $|\alpha| = 1$, which are obtained intuitively from Fig. 6(a) by shifting the voluntary effort. Setting $|\alpha| > 1$ generates counter-acting wrenches, c.f. Fig. 4 (b).

3.4 Dyadic allocation of roles

The effort sharing policies (17) with constant policy parameter α imply a *static role* in terms of the effort sharing ratio among the dyad in the redundant direction, resulting from a feedforward calculation of the agents' applied wrenches. In contrast, a *dynamic role* allocation strategy as investigated here varies the policy parameter α over time depending on the measured *wrench feedback of the partner*. In the dyadic case, the robotic agent may compute an estimation of its partner's applied wrench, if the object's dynamics (1) and kinematics (4), (5) is known to the robot. In Section 4.1 we provide details on such an estimation strategy.

Note: The roles and the allocation strategy refer to a task's redundant degree of freedom. With multiple redundant degrees of freedom, role allocations between the partners may differ.

The resulting robot behavior in terms of its urge to complete the task is influenced by the velocity profile of the configuration trajectories planned by the robot. Velocity profiles can be taken from observations in human-human experiments, can describe the technical limitations of the robotic system in its environment, or can be a mixture of both. Kinodynamic motion planning techniques can be alternatively used to produce trajectories with bounds on velocities and accelerations (Donald et al., 1993) in order to generalize the approach to arbitrary feasible transport tasks.

3.4.1 Constant role allocation

As a baseline strategy, we propose a constant allocation of roles during the task. Any arbitrary choice of a constant parameter α directly affects the robot's urge to accomplish the task.

Given a certain velocity profile, following the inverse dynamics a choice of $\alpha = 0$ results in an equal, feedforward composition of the external wrench in the redundant degree of freedom. In the performed human user studies we investigate this case as it is symmetric: A human partner applying the same wrench as the robot in the redundant degree of freedom moves the object according to the robot's velocity profile. In contrast, a human partner who applies the same wrench in the opposite direction cancels the robot's applied wrench.

3.4.2 Weighted proactive role allocation

For the realization of the weighted role allocation strategy developed in this work, we propose a continuous, first order dynamical system with the policy parameter

$$\alpha = \alpha_0 + \int_{t_0}^{t} \dot{\alpha} dt, \tag{18}$$

bounded within the interval $[-1, 1]$ by an anti-windup saturation to obtain only the efficient policies. The derivative

$$\dot{\alpha} = \begin{cases} \tau_{-,w} \left| \tilde{u}^C_{1,y,est} \right|, & \text{if } \xi = 0 \\ \tau_{+,w} \, \tilde{u}^C_{y,thr}, & \text{if } \xi = 1 \wedge \left| \tilde{u}^C_{1,y,est} \right| < \tilde{u}^C_{y,thr} \\ \tau_{+,w} \left| \tilde{u}^C_{1,y,est} \right| & \text{otherwise} \end{cases}$$

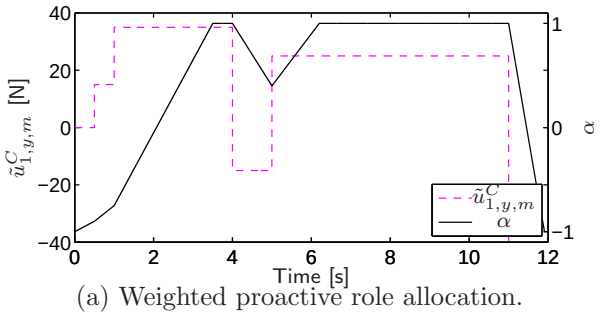

(a) Weighted proactive role allocation.

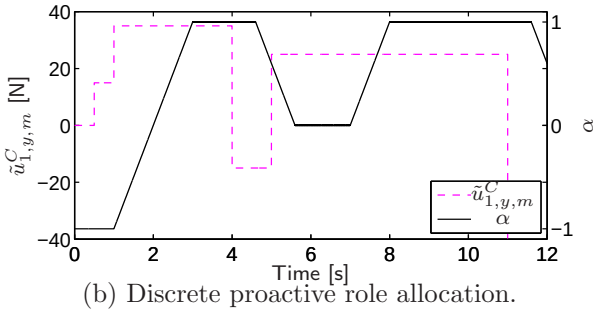

(b) Discrete proactive role allocation.

Figure 7: Policy parameter α over time for a simulated profile of the human wrench component $\tilde{u}^C_{1,y,m}$ and an expected wrench component $\tilde{u}^C_{1,y} > 0$.

is weighed by the feedback of the human wrench component $\tilde{u}^C_{1,y,est}$ in the redundant direction, which yields a role allocation with a progressively changing policy depending on the magnitude of the partner's contribution, and the agreement indicator

$$\xi = \begin{cases} 0, & \text{if } \operatorname{sgn}(\tilde{u}^C_{1,y}) \neq \operatorname{sgn}(\tilde{u}^C_{1,y,est}) \neq 0 \\ 1, & \text{otherwise.} \end{cases} \tag{19}$$

Note that the initial value $\alpha_0 = -1$ produces initially a minimum-robot-effort behavior. Either zero human force input or force input $\tilde{u}^C_{1,y,est}$ in the expected direction $\operatorname{sgn}(\tilde{u}^C_{1,y})$ produces an agreement value of $\xi = 1$ and lets the policy parameter α rise which leads to emerging robot effort. A threshold $\tilde{u}^C_{y,thr}$ is used to define a neutral human force input which is treated as silent agreement. The constants $\tau_{-,w}$ and $\tau_{+,w}$ weigh the human's agreement or disagreement force input. A faster reaction to dis-

agreement signals (i.e. $-\tau_{-,w} > \tau_{+,w} > 0$) is considered to be a reasonable option. This choice lets the robot rapidly fall back to minimum effort if the human signals discomfort by applying a counteracting force. The qualitative dynamical behavior of the weighted role allocation scheme is illustrated by a simulation example in Fig. 7(a).

3.4.3 Discrete role allocation

In order to investigate whether role allocation with a small number of distinct meaningful steps is more understandable for the human partner and hence beneficial for cooperation, a discrete version of the continuous role allocation mechanism is developed. A chattering-free output discretization of the weighted role allocation mechanism to three distinct values $\zeta = \{-1, 0, 1\}$ is achieved by an output quantization with hysteresis. The rate of change of the internal continuous policy parameter $\hat{\alpha}$ is also chosen depending on the agreement indicator ξ from (19) with

$$\dot{\hat{\alpha}} = \begin{cases} \tau_{+,d}, & \text{if } \xi = 1 \\ \tau_{-,d}, & \text{otherwise.} \end{cases}$$

A quantization with hysteresis maps the internal continuous policy parameter $\hat{\alpha}$ onto the discrete value ζ, replacing the continuous output (18). A smooth transition between the three discrete levels is achieved by a bang-bang-like ramp generating mechanism

$$\dot{\alpha} = \tau_b \operatorname{sgn}(\zeta - \alpha)$$

where τ_b denotes a blending time constant. The qualitative behavior of the discrete role allocation scheme is also illustrated by simulation, see example in Fig. 7(b).

4 Robot interaction control

In order to embed the role behavior developed in Section 3 in a robotic agent, we present an architecture for feedback interaction control, see Fig. 8. The robot's applied wrench $\tilde{\boldsymbol{u}}_2$ is realized by an admittance-type force controller imposing motion at the robot's grasp point $\boldsymbol{x}_2$ on the object. The effort-role behavior (grey box) consisting of three modules, role allocation, sharing policy and sharing strategy generates the robot's input behavior for given external wrenches $\hat{\boldsymbol{u}}_c$ and estimates of the human applied wrench $\tilde{\boldsymbol{u}}_{1,est}$. A given object-related trajectory $\boldsymbol{x}_{c,d}$ is reference to the system's inverse dynamics comprising a model of the object as well as the robot, and generates a feedforward component of the external wrench $\hat{\boldsymbol{u}}_{c,dyn}$. A feedback component $\hat{\boldsymbol{u}}_{c,imp}$ as output of an impedance control law ensures tracking of the object configuration under model uncertainties and unexpected human behavior. In the following section, the interaction control architecture is explained in detail.

4.1 Estimation of the partner's input

The robotic agent may compute an estimate of the applied wrench of a single human partner. If the robot's kinesthetic feedback available through its end effector with a rigid grasp at $\boldsymbol{x}_2$ is sufficiently accurate, i.e. it provides measurements $(\boldsymbol{x}_2, \dot{\boldsymbol{x}}_2, \ddot{\boldsymbol{x}}_2)$ of the grasp point's configuration, the object's motion $(\boldsymbol{x}_c, \dot{\boldsymbol{x}}_c, \ddot{\boldsymbol{x}}_c)$ can be inferred by the robot's partial grasp matrix $\boldsymbol{G}_2^T$, which is invertible for a rigid grasp. In the dyadic case, the external wrench is superposed by the partners' wrench components according to (3), c.f. $\boldsymbol{u}_c = \boldsymbol{u}_{c,1} + \boldsymbol{u}_{c,2}$ in Fig. 8. Thus, we obtain the estimated applied wrench

$$\tilde{\boldsymbol{u}}_{1,est} = \boldsymbol{G}_1^{-1} \left(\boldsymbol{u}_c - \boldsymbol{G}_2 \tilde{\boldsymbol{u}}_{2,m} \right), \tag{20}$$

where the external wrench $\boldsymbol{u}_c$ is calculated using the inverse dynamics[1] (1), $\tilde{\boldsymbol{u}}_{2,m}$ is the measured applied wrench of the robot and $\boldsymbol{G}_1$ is the human's partial grasp matrix. Due to the superposition of external wrench components (3), only a single agent's unknown input can be determined uniquely by (20).

4.2 Admittance-type force control

An admittance-type force control law is utilized to impose the robot's applied wrench $\tilde{\boldsymbol{u}}_2$. The controller

[1] Certain non-linearities such as static friction prevent invertibility of the object dynamics and therefore the partner's input estimation.

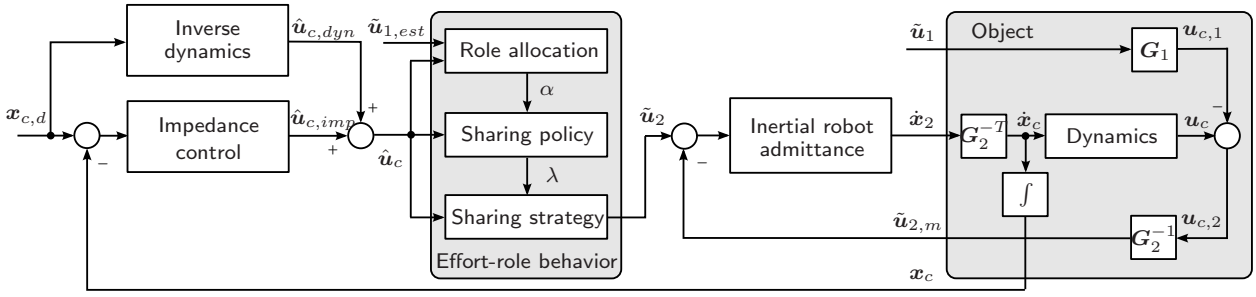

Figure 8: Overall scheme of the interaction control architecture embedding the effort-role behavior.

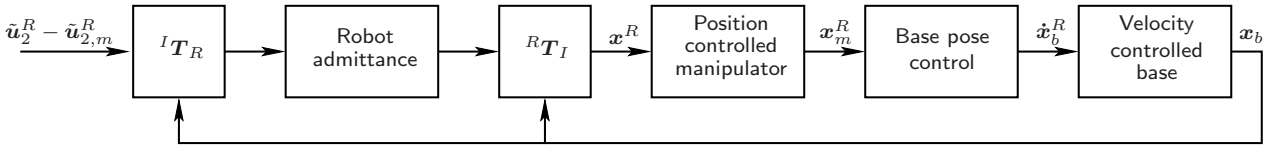

Figure 9: Inertial admittance-type control scheme including manipulator-base coordination.

renders the dynamics

$$\boldsymbol{u}_2 - \boldsymbol{u}_{2,m} = \boldsymbol{M}_r \ddot{\boldsymbol{x}}_{\boldsymbol{2}} + \boldsymbol{D}_r \dot{\boldsymbol{x}}_2, \tag{21}$$

where $\boldsymbol{u}_{2,m}$ is the measured input wrench, matrix $\boldsymbol{M}_r$ and $\boldsymbol{D}_r$ are a rendered virtual robot's mass and friction respectively. Note that for a rigid grasp, (21) has to be formulated in $\dim(\boldsymbol{u}_2)$. Zeroing ineffective components of $\boldsymbol{u}_2$ (e.g. $\boldsymbol{u}_{2,\phi} = 0$) yields the robot's applied wrench $\tilde{\boldsymbol{u}}_2$. In order to make use of the extended workspace of a mobile robot composed by a manipulator-base system, the admittance control law is calculated in the inertial frame similar to Unterhinninghofen et al. (2008). The control scheme depicted in Fig. 9 compensates for repositioning of the mobile base through transformations between the local robot frame R and the inertial frame, which are denoted by ${}^I\boldsymbol{T}_R$ and ${}^R\boldsymbol{T}_I$ respectively, so that the grasp pose of the manipulator is not affected.

Following of the mobile base is ensured by the velocity command $\dot{\boldsymbol{x}}_b^R = \begin{pmatrix} \dot{x}_{b,\phi} & \dot{x}_{b,x} & \dot{x}_{b,y} \end{pmatrix}^T$ generated according to the control law

$$\dot{\boldsymbol{x}}_b^R = \operatorname{diag}\left(K_{hdg}, K_{dst}, K_{tng}\right) \begin{pmatrix} e_{hdg} & e_{dst} & e_{tng} \end{pmatrix}^T. \tag{22}$$

Three independent proportional controllers with gains K_{hdg}, K_{dst} and K_{tng} move the mobile base controlling heading error e_{hdg}, distance error e_{dst} and tangential error e_{tng} to zero with respect to a desired relative configuration of the manipulated object and the robot base, as illustrated in Fig. 10. The desired pose of the end-effector $\boldsymbol{x}_d^R$ w.r.t. the robot frame R is chosen to meet a certain lower bound μ_{min} of the manipulability measure

$$\sqrt{\det\left(\boldsymbol{J}^T\boldsymbol{J}\right)} > \mu_{min} \quad \forall \left\|\boldsymbol{x}_d^R - \boldsymbol{x}_m^R\right\| < \Delta\boldsymbol{x}^R,$$

where $\boldsymbol{J}$ is the Jacobian of the manipulator and $\Delta\boldsymbol{x}^R$ describes required workspace bounds during manipulation. Assuming a rigid grasp of the robot's manipulator on the object, the errors e_{hdg}, e_{dst} and e_{tng} can be determined as a function of $\boldsymbol{x}_d^R$ and $\boldsymbol{x}_m^R$. The control gains in (22) are tuned to achieve a smoothly-damped, spring-like following behavior of the platform that keeps the manipulator within its workspace bounds during mobile manipulation. The resulting motion command $\dot{\boldsymbol{x}}_b^R$ is then executed by an omni-directional velocity control law as proposed in Nitzsche et al. (2003).

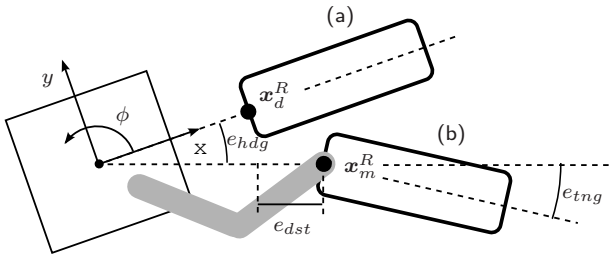

Figure 10: (a) Desired and (b) actual configuration of the base w.r.t. the object, described by a desired and measured pose of the manipulator's end-effector, $\boldsymbol{x}_d^R$ and $\boldsymbol{x}_m^R$ respectively.

4.3 Object-centered motion tracking

In addition to the capability to apply input wrenches $\tilde{\boldsymbol{u}}_2$ on the manipulated object, the mobile robotic agent needs the capability to impose a desired trajectory of the object configuration $\boldsymbol{x}_{c,d}$ as a result of the shared plan. The tracking behavior is synthesized in an object-centered representation by means of an external wrench

$$\hat{\boldsymbol{u}}_c = \hat{\boldsymbol{u}}_{c,dyn} + \hat{\boldsymbol{u}}_{c,imp}, \tag{23}$$

decomposed by the underlying effort-behavior. Wrench component $\hat{\boldsymbol{u}}_{c,dyn}$ compensates in a feed-forward branch for the dynamics of the combined manipulator-object system with

$$\hat{\boldsymbol{u}}_{c,dyn} = \boldsymbol{M}(\boldsymbol{x}_c, \dot{\boldsymbol{x}}_{c,d})\ddot{\boldsymbol{x}}_{c,d} + \boldsymbol{f}(\boldsymbol{x}_c, \dot{\boldsymbol{x}}_{c,d}), \tag{24}$$

where mass matrix $\boldsymbol{M}(\boldsymbol{x}_c, \dot{\boldsymbol{x}}_{c,d})$ and friction term $\boldsymbol{f}(\boldsymbol{x}_c, \dot{\boldsymbol{x}}_{c,d})$ comprise the mass and friction terms from (1) and (21). An object-centered impedance-type control law acting on the tracking error of the configuration $\boldsymbol{x}_c$ generates the external wrench component

$$\hat{\boldsymbol{u}}_{c,imp} = \boldsymbol{K}_p(\boldsymbol{x}_{c,d} - \boldsymbol{x}_c) + \boldsymbol{K}_d(\dot{\boldsymbol{x}}_{c,d} - \dot{\boldsymbol{x}}_c). \tag{25}$$

Stiffness gain $\boldsymbol{K}_p$ and damping gain $\boldsymbol{K}_d$ render a compliant behavior, if the object configuration deviates from the expected.

The external wrench (23) guaranteeing object-centered motion tracking feeds the effort-role behavior, which can be regarded as a selective wrench filter. Depending on the estimated human's applied wrench $\tilde{\boldsymbol{u}}_{1,est}$ and the policy parameter α of the role allocation scheme, the robot's applied wrench $\tilde{\boldsymbol{u}}_2$ reflects the robot's voluntary contribution to the task effort as a result of the effort-role behavior. The admittance-type force control law (21) imposes the applied wrench on the object and renders the robot's input behavior.

5 Experiment

In order to evaluate our effort sharing strategy and the effects of the role allocation schemes developed in Section 3.4, we conducted a user study at Munich *Multi Joint Action Laboratory* of *CoTeSys* research center. A human-robot interaction scenario was designed for this study in a unique large-scale setup, involving the joint manipulation of a real-sized bulky object. The participants were asked to maneuver jointly with a human-sized mobile robot through our cluttered lab area (see Fig. 1) in order to collaboratively transport a table. The realization of such a joint action task serves as the proof of concept for our approach and provides valuable observations through a real scenario. In this section, we describe the experimental setup, conditions, design, and the procedure.

5.1 Experimental setup

The mobile robot used in the experiment consists of an omni-directional mobile base developed by Hanebeck et al. (1999), two admittance-controlled anthropomorphic manipulators (Stanczyk and Buss, 2004) using 6-degrees-of-freedom wrench sensors (*JR3 67M25A3-I40-DH*) on each end effector. A two-finger parallel gripper of type *Schunk PG70*, which is mounted at the robot's right manipulator, provided a rigid grasp of the flange attached to the table. A detailed description of the robot's system hardware and software architecture can be found in (Althoff et al., 2009; Medina et al., 2011). During the experiment all data collection was done by the mobile robot at a sampling frequency of 1 kHz. The wrench sensor at the human-side was identical to those attached to the end effectors of the robot and it was connected to a PC on the robot. The table configuration as well

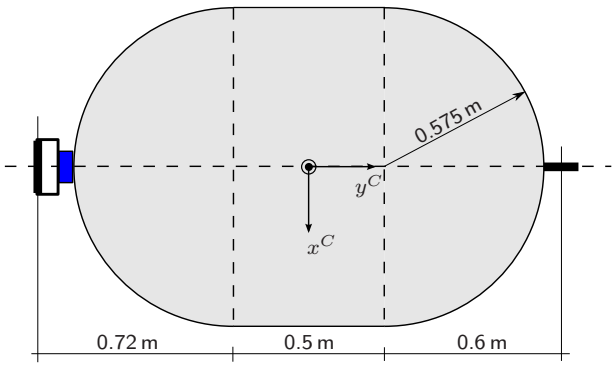

Figure 11: Cooperatively manipulated table equipped with a handle and wrench sensor for the human (left) and a grasp flange for the robot (right), both mounted at a height of 0.925 m over the ground.

as the grasp points were tracked using the robot's inverse kinematics, transformed by the mobile base's odometry readings. The interaction control architecture was implemented in *MATLAB Simulink* and executed at 1 kHz under *Ubuntu Linux* utilizing *Matlab's Real-Time Workshop*.

During the experiment, the subjects were asked to move a wooden table weighing 44 kg that was mounted on an aluminum frame standing on ball-caster feet (see Fig. 1). The ball casters provided low-friction, holonomic maneuverability of the table. A handle and a flange were rigidly attached to the table at facing sides for the grasp points of the human and the robot, respectively (see Fig. 11). The flange was a solid wooden plate that provided slippage free zero-backlash grasp for the robot.

The parameters used by the robot's interaction control architecture (21) and (25) in Section 4 were set to the following values regarding the task-relevant degrees of freedom:

$$\begin{aligned}
\boldsymbol{M}_r &= \mathrm{diag}(0.4\,\mathrm{kgm}^2, 20\,\mathrm{kg}, 20\,\mathrm{kg}) \\
\boldsymbol{D}_r &= \mathrm{diag}(10\,\mathrm{Nmsrad}^{-1}, 100\,\mathrm{Nsm}^{-1}, 100\,\mathrm{Nsm}^{-1}) \\
\boldsymbol{K}_p &= \mathrm{diag}(200\,\mathrm{Nrad}^{-1}, 200\,\mathrm{Nm}^{-1}, 200\,\mathrm{Nm}^{-1}) \\
\boldsymbol{K}_d &= \mathrm{diag}(50\,\mathrm{Nmsrad}^{-1}, 50\,\mathrm{Nsm}^{-1}, 50\,\mathrm{Nsm}^{-1})
\end{aligned}$$

An off-line estimation of the object dynamics used in (24) revealed the parameters of the table mass matrix

$$\boldsymbol{M}_c = \mathrm{diag}(13.5\,\mathrm{kgm}^2, 44\,\mathrm{kg}, 44\,\mathrm{kg}),$$

the table friction $\boldsymbol{f}_c$ was considered as a Coulomb-type friction of 14 N in total, acting at the table feet.

5.2 Conditions

We designed three conditions implementing different behaviors of the robot:

1. *Constant Role Allocation (CRA):* As explained in Section 3.4.1, the robot contributes to the task without changing its role, i.e. it uses a balanced-effort policy $\alpha = 0$ at all times.

2. *Weighted Proactive Role Allocation (WPRA):* As explained in Section 3.4.2, as long as the force applied by the human is in the expected direction, or the human is inactive, the robot increases the policy parameter α gradually with time. Otherwise, it decreases α. During the experiment, we used $\tau_{+,w} = 0.02\,(\mathrm{Ns})^{-1}$, $\tau_{-,w} = -0.04\,(\mathrm{Ns})^{-1}$, and $\tilde{u}^C_{1,y,thr} = 10\,\mathrm{N}$.

3. *Discrete Proactive Role Allocation (DPRA):* Similar to WPRA, the robot changes its role by increasing or decreasing α gradually. We defined three discrete roles in this condition (see Section 3.4.3). During the experiment, we used $\tau_{+,d} = 0.2\,\mathrm{s}^{-1}$, $\tau_{-,d} = -2\,\mathrm{s}^{-1}$, and $\tau_b = 2\,\mathrm{s}^{-1}$.

5.3 Participants, procedure and design

18 subjects (6 female and 12 male), aged between 19 and 44, participated in our study. All the subjects were right handed and used their right hands for moving the table. We conducted a within subjects experiment, in which each subject experimented with all conditions in a single day. The conditions (CRA, WPRA, and DPRA) were presented to the subjects in permuted order using a balanced Latin Square design to avoid learning effects. The subjects

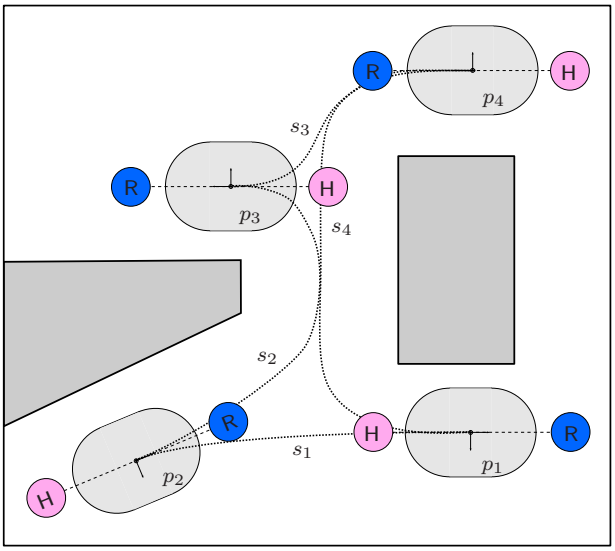

Figure 12: Bird's eye view of the lab area used for the experiments. The outer box corresponds to the boundary of the environment and spans a square of approximately $8\,\mathrm{m} \times 8\,\mathrm{m}$. The regions marked as gray are occupied by obstacles. The positions of the table and the interacting dyad (i.e. the human and the robot) in each of four designated parking configurations, $p_i, i = 1..4$, are depicted. The paths, $s_i, i = 1..4$, connecting the parking configurations are represented by dotted lines.

were given detailed instructions about the task and the conditions before the experiment.

In the experiment, a trial consisted of moving the table jointly with the robot to four parking configurations and then coming back to the initial configuration, as shown in Fig. 12. The subjects were allowed to apply pushing and pulling forces using only their dominant hands by holding the handle of the table; lifting the table off the ground and talking during the experiment were prohibited. The positions of the human and the robot in each of the parking configurations were clearly marked on the floor of the area. These marks were shown to the subjects before the experiment. The free space available for maneuvering the table between the parking configurations was constrained by obstacles in such a way that ambiguities and possible alternative common paths were avoided. Extension 1 provides the reader with a video of an experimental trial's course.

For each condition, the subjects performed the task three times (i.e. three trials). After each trial, a small break was given to initialize the table and robot pose. After performing these three trials successfully, the subjects were given a questionnaire to comment on their experience. Afterwards, they were presented with a new condition.

6 Evaluation

In this section, quantitative as well as subjective measures used for the evaluation of the user study are introduced.

6.1 Quantitative measures

This section presents details on the quantitative measures we adopt in analysis. The data collected in the first 300 ms of each trial is discarded to eliminate possible discrepancies encountered at the beginning of the trials. Also data collected at the final leg of segment s_4 (see Fig. 12) is discarded since the final parking procedure was difficult for some of the participants, and we had to cut some trials early due to impending collisions with obstacles. The data is low-pass filtered using a first-order filter with 15 Hz cut-off frequency.

Task performance is quantified in terms of task completion time. We also examine the individual interaction forces applied by the agents, the work done by the partners, and the total work done on the table as indication of the physical effort. Also, the degree of cooperation under each condition is investigated with respect to the amount of disagreement in the dyad's operation and the distribution of the robot's effort policy.

6.1.1 Task performance

The completion time (CT) of each trial is taken as a measure of performance.

6.1.2 Effort

The average of the human's and robot's applied wrenches and the work done by them are considered to be indications of the *effort* made by the agents. Work done by the agents during a trial is calculated by

$$W_i = \int_0^{CT} |\tilde{\boldsymbol{u}}_{i,m} \cdot \dot{\boldsymbol{x}}_i| \, dt,$$

where $\tilde{\boldsymbol{u}}_{i,m}$ denotes the measured wrench exerted by the agent and $\dot{\boldsymbol{x}}_i$ the velocity of the grasp point. The total work done on the table by the partners during a trial considers the accumulated energy transfer on the table, i.e. how efficiently the table could be moved to the parking configurations. It is calculated by

$$W_{table} = \int_0^{CT} |\boldsymbol{u}_c \cdot \dot{\boldsymbol{x}}_c| \, dt,$$

where the motion-causing external wrench $\boldsymbol{u}_c$ is obtained by evaluating (3) for $\tilde{\boldsymbol{u}}_{i,m}$. Note that the absolute energy flow is accumulated, since the human partner is assumed not to recoup by absorbing energy, i.e. through breaking actions.

6.1.3 Amount of disagreement

In our experiment, a disagreement is assumed to occur when two partners pull or push the table in opposite directions along the y^C-axis. Instead of contributing to the movement of the object, part of the forces in this axis are wasted for compressing the table (i.e. squeeze force) or resisting the other partner (i.e. tensile force). Groten et al. (2009) call these forces interactive forces defined as

$$u_I = \begin{cases} \tilde{u}^C_{1,y}, & \text{if } \operatorname{sgn}(\tilde{u}^C_{1,y}) \neq \operatorname{sgn}(\tilde{u}^C_{2,y}) \\ & \wedge\, |\tilde{u}^C_{1,y}| \leq |\tilde{u}^C_{2,y}| \\ -\tilde{u}^C_{2,y}, & \text{if } \operatorname{sgn}(\tilde{u}^C_{1,y}) \neq \operatorname{sgn}(\tilde{u}^C_{2,y}) \\ & \wedge\, |\tilde{u}^C_{1,y}| > |\tilde{u}^C_{2,y}| \\ 0, & \text{otherwise.} \end{cases}$$

In order to come up with a metric of disagreement, the interactive forces during the disagreement periods are weighed with the time spent in disagreement. Since we are not interested whether the agents disagree by pushing or pulling against each other (which is indicated by sign of u_I), the *amount of disagreement*

$$ADI = \int_0^{CT} |u_I| \, dt,$$

is calculated based on the magnitude of the interactive forces.

6.1.4 Role allocation

The *frequency distribution* of the policy parameter α is investigated to provide a better understanding of the dynamic role allocation behaviors in different conditions.

6.2 Subjective measures

At the end of each condition, the subjects are asked to fill in a questionnaire, which is designed with the technique that Basdogan et al. (2000) have used in the past for investigating haptic collaboration in shared virtual environments. The questionnaire consists of 20 questions taken from NASA-TLX task load index (Hart and Stavenland, 1988) as well as those developed by Kucukyilmaz et al. (2011). The subjects indicate their level of agreement or disagreement on a 7-point Likert scale for a series of questions, some of which are rephrased and asked again within the questionnaire in an arbitrary order. The average of the subjects responses to the rephrased questions is used for the evaluation. NASA-TLX evaluates the degree to which each of the following six factors contribute to the task workload:

- *Mental Demand:* One question asks how much mental and perceptual activity was required for achieving the task (e.g. thinking, deciding, calculating, remembering, looking, searching, etc.).
- *Physical Demand:* One question asks how much physical activity was required for achieving the task (e.g. pulling, pushing, turning, calculating, remembering, looking, searching, etc.).
- *Temporal Demand:* One question asks how much time pressure the subjects felt during the task.

- *Performance:* One question asks the subjects to assess their self-performance in accomplishing the goals of the task.

- *Effort:* One question asks how hard the subjects had to work to accomplish their level of performance.

- *Frustration Level:* One question asks how much irritation, stress or annoyance the subjects felt during the task.

The remaining questions are asked in the following categories:

- *Collaboration:* Two questions investigate the extent to which the subjects had a sense of collaborating with the robot during the task.

- *Interaction:* Two questions explored the level of interaction the subjects experience during the task.

- *Comfort:* One question asks how comfortable the task was.

- *Pleasure:* One question asks how pleasurable the task was.

- *Degree of Control:* Two questions ask the subjects about their perceived degree of control on the movement of the table.

- *Predictability:* Two questions investigate how predictable the robot's movements were during the task.

- *Trust:* Two questions investigate whether the subjects trusted their robotic partner on controlling the table or not.

- *Human-likeness:* Two questions ask the subjects whether the robot's actions (movement patterns) resembled those of a human being acting in a similar real-life scenario.

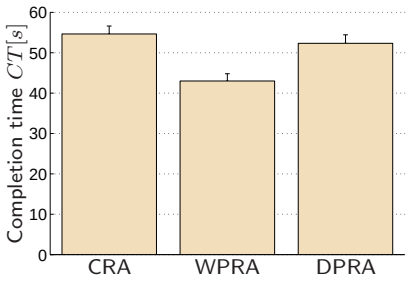

Figure 13: Average completion time of the task. The bars represent standard errors of the means.

7 Results

This section presents the results of the experiment in terms of the quantitative and subjective measures defined in Section 6. Statistically significant differences between conditions were investigated using one way repeated measures ANOVA and multiple comparisons were performed via post-hoc t-tests with Bonferroni correction. Mauchly's test was conducted to check if the assumption of sphericity was violated. If so, the degrees of freedom were corrected using Huynh-Feldt estimates of sphericity.

7.1 Quantitative analysis

In this section, we present the quantitative results according to the measures introduced in Section 6.1.

7.1.1 Task performance

Fig. 13 illustrates the mean completion time under each condition and the standard error of the means.

According to ANOVA results, we observe a statistically significant effect of the condition on completion time ($p < 0.001$). Specifically, the subjects completed the task significantly faster under WPRA than they did under the other two conditions. While the completion time is slightly smaller in DPRA than it is in CRA, the difference between these conditions is not significant.

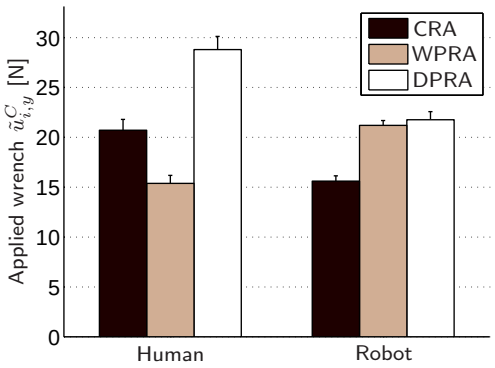

Figure 14: The averaged applied wrenches of the human and the robot. The bars represent standard errors of the means.

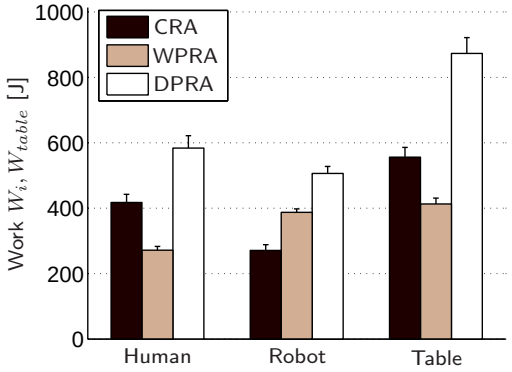

Figure 15: Average work done by individual agents and average work done on the table. The bars represent standard errors of the means.

7.1.2 Effort

Fig. 14 illustrates the mean individual wrenches applied by the agents and the standard error of the means.

According to ANOVA results, the experimental condition has a significant effect on interaction forces of both the human and the robot ($p < 0.001$). We observe that the average wrench applied by the human under WPRA is significantly smaller than it is under the other conditions ($p < 0.001$), whereas it is significantly higher under DPRA ($p < 0.001$). On the other hand, the applied wrench of the robot is significantly higher under WPRA and DPRA than it is under CRA ($p < 0.001$).

Fig. 15 illustrates the average work done by the individual agents and the dyad under each condition. The error bars denote the standard error of the means. The results are in parallel to those observed for the wrenches applied by the agents.

We consider the work done as an indication of physical effort. ANOVA results suggest that there is a significant effect of the experimental condition on the individual work done by the agents and the work done on the table ($p < 0.001$). We observe that the subjects put the least effort under WPRA ($p < 0.001$) and the most under DPRA ($p < 0.001$). Similarly, we observe that the total work done on the table under WPRA is smaller than that under CRA ($p < 0.05$) and DPRA ($p < 0.001$). The total work is the largest under DPRA ($p < 0.001$). The robot showed significantly more effort under WPRA and DPRA than it did under CRA ($p < 0.001$). Even though we observe the highest robot effort in DPRA, the difference between the WPRA and DPRA conditions is not statistically significant.

7.1.3 Amount of disagreement

The amount of disagreement under each condition is illustrated in Fig. 16. The ANOVA results indicate a significant effect of the condition on the amount of disagreement ($p < 0.05$). The multiple comparison results imply that the amount of disagreement is similar under CRA and WPRA, whereas it is lower under DPRA than CRA ($p < 0.001$) and WPRA ($p < 0.001$). Note that we consider only the signs of the applied wrenches to decide whether there is a disagreement between the partners. Also we check for interactive forces that are smaller than 1 N, and do not treat these as disagreements.

7.1.4 Role allocation

Fig. 17 illustrates how the role allocation behavior changes for the WPRA and DPRA conditions. For

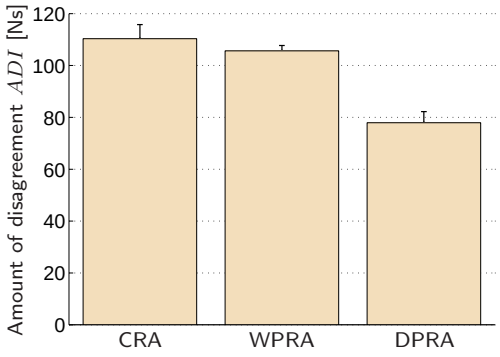

Figure 16: The averaged amount of disagreement under each condition. The bars represent standard errors of the means.

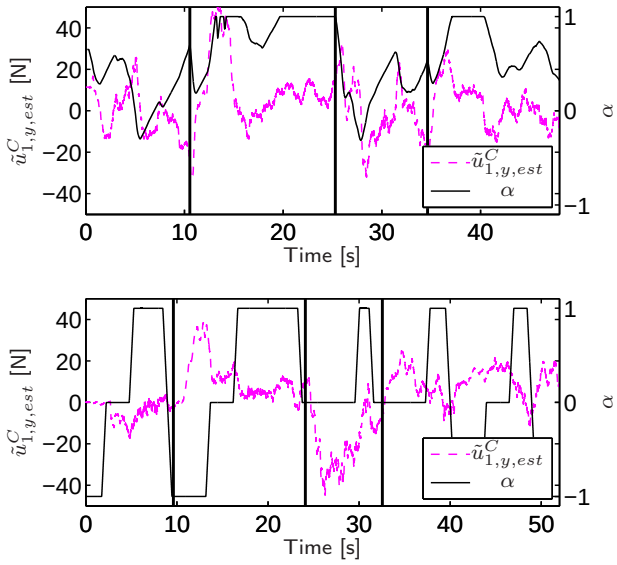

Figure 17: Sample trials for conditions WPRA (top) and DPRA (bottom). The straight lines denote the policy parameter α, and the dashed lines denote the component $\tilde{u}^C_{1,y,est}$ of the human's wrench profile. Task segments are separated by vertical bold lines.

each condition, a sample trial is selected showing the human's wrench profile and the resulting profile of the policy parameter α. Upon examining the plots, we observe that even though the human's wrench profile is similar under WPRA and DPRA, the resulting robot behavior is drastically different. In particular, the discrete state transitions under DPRA become obvious in contrast to the continuous blending under WPRA.

The frequency distributions of the policy parameter α under the WPRA and DPRA conditions are illustrated in Fig. 18. We observe that under WPRA the robot acted towards maximum effort. On the other hand, we see a almost uniform distribution between the three discrete states of effort sharing behaviors (also due to transitions, we notice values in between these three states).

7.2 Subjective evaluation

The key results of the subjective evaluation are as follows:

- The subjects thought that the task was physically and mentally less demanding under WPRA. The physical demand for DPRA was significantly higher than it was for WPRA ($p < 0.005$) and CRA ($p < 0.05$).
- The subjects felt significantly less comfortable under DPRA than they felt under CRA ($p < 0.01$) and WPRA ($p < 0.005$).
- The subjects believed that their control over the table's movements under DPRA was significantly more than that under WPRA ($p < 0.05$).
- Under DPRA, the predictability of the robot was significantly lower than it was under CRA ($p < 0.05$).

Fig. 19 shows the mean values of the subjects' responses to the questionnaire and the standard error of the means.

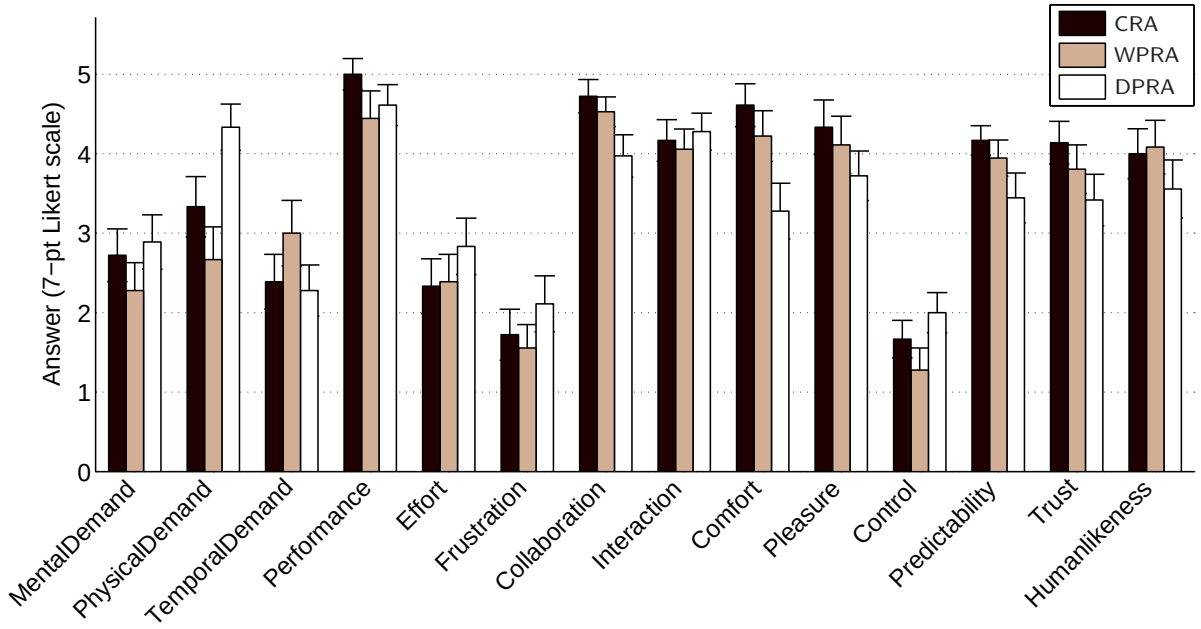

Figure 19: Means of the subjective measures in each condition. The bars represent standard errors of the means.

8 Discussion

In this study, we investigate the benefits of using a dynamic role allocation scheme for cooperative human-robot interaction. We implemented two different dynamic role allocation schemes, i.e. WPRA and DPRA, and compared them to a scheme with constant role allocation, i.e. CRA. The evaluation of cooperative physical human-robot interaction is especially tricky due to the diversity of real life applications and target domains. In such systems, optimizing for the human's collaborative experience as well as the task performance is desired. In order to present a broad analysis, we utilized quantitative and subjective measures as explained in Section 6, each of which is designed to evaluate a different aspect of the cooperative task. Along with performance measures, we propose quantitative measures for evaluating the effort and efficiency of the partners in the dyadic task. Subjective measures are presented to discover the acceptability of the proposed schemes by the humans. However, our results indicate that no single interaction scheme can satisfy every aspect of interaction. Hence, the domain and task knowledge should be considered carefully.

The subjective evaluation, when considered along with the quantitative results presents insight about the users' perception of different effort sharing policies. During the experiments, we observed that, under DPRA, the subjects accelerated and decelerated from time to time as an effect of adaptation to the changing policy α. We infer that such movements might have caused the subjects to finish the task in a longer time. The average wrench of the robot is significantly higher under WPRA and DPRA than it is under CRA, which indicates a possible tendency towards maximum effort in the robot's behavior under both conditions. As a consequence of the smooth blending, under WPRA, the maximum effort policy that was dominantly employed by the robot made the subjects think that the task required them to be faster (i.e. the task had a higher temporal demand).

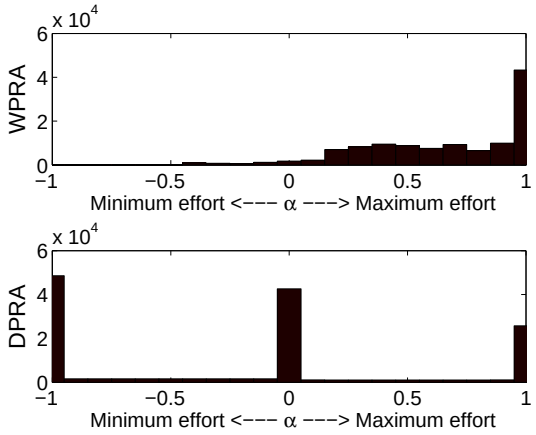

Figure 18: The frequency distribution of the policy parameter α under each condition.

Eventually this perception could be responsible for the lower completion time under WPRA.

We observed that the level of agreement during the task was the highest under DPRA. Reed et al. (2005) mention that sometimes force oscillations may be observed during interaction for negotiation purposes or in an effort to adapt to the varying velocity enforced by the robot. Since the states were discrete under DPRA, the behavior of the robot was observable. Hence the users might have needed to use force oscillations less for adaptation, but acted in a more determinate way through their applied forces, resulting in an increased level of agreement during the task.

Under DPRA, the subjects were able to observe the operation of the robot more clearly and infer that different behaviors were displayed by the robot. On the other hand, WPRA resulted in smooth role blending, which was not consciously perceived by the subjects for most of the time. We also observe that the mental and physical demand of task, as well as the frustration level and the physical effort were higher under DPRA. This may be an artifact of the pronounced role switching behavior faced during the task under DPRA.

The subjects thought that the robot was acting less collaboratively under WPRA and DPRA. A possible reason for this is that the changing effort role of the robot made the interaction more complex, and the subjects favored a constant role allocation scheme. The subjects found the level of interaction to be higher under DPRA. Under WPRA, the role exchanges were probably too smooth to be observable, hence the subjects failed to perceive the interactive nature of the task.

The subjects felt in control of moving the table under DPRA significantly more than they did under WPRA. They also thought that they spent more effort in DPRA, which agrees with our effort measures. Also since the robot displayed greater effort under WPRA, the perception of the relative control level of the subjects might have dropped. Additionally, the subjects felt significantly less comfortable under DPRA and they thought that the predictability of the robot was significantly lower than it was under CRA. Since the behavior of the robot was less smooth under DPRA, the subjects might have felt discomfort due to abrupt role transitions and experienced a difficult time in inferring the robot's actions in advance. However, in WPRA, as the behavior was smooth, the subjects were able to predict the robot's actions better. As the subjects could not infer the actions of the robot clearly under DPRA, they may be driven to being more dominant in pulling and pushing the table, which eventually increases their perceived control level during the task.

The subjects' belief that the robot would perform the task correctly was the highest under CRA, in which the subjects observed no unexpected behaviors as the robot's effort sharing policy was constant at all times. Finally, the human-likeness of the robot was lower under DPRA than it was under WPRA and CRA. As mentioned above, we observed that the smooth operation under CRA and WPRA provides a more comfortable experience for the subjects, in which the subjects reported that they could trust the robot and predict its actions. Even though we have not yet discovered the salient features that make the communication with a robot more human-like, obviously subjective sensations such as smoothness, comfort, predictability, and trust adds to higher human-likeness scores.

The aforementioned points draw a clear distinction between two different implementations of a dynamic role allocation scheme. Although in essence both WPRA and DPRA realize dynamic role allocation based on the wrench acquired from the same human partner, the discretized version of the scheme invoke more distinct role transitions. However, these defined transitions increase the visibility of the underlying scheme, and allow the users of the system to observe it better. This makes a DPRA-like scheme a viable alternative for interactive training applications. In training, it is necessary for the users to observe the role of the trainer (i.e. the robot) so that they can adapt to it. When the trainer's role is not perceived, the users typically tend to obey the guiding system and do not learn the dynamics of the system (Forsyth and Maclean, 2006). This effect can clearly be observed when we examine the frequency distribution of the policy parameter in Fig. 18. As indicated in the figure, under WPRA, the users tend to go along under the supervision of the robot most of the time. Since the robot puts its maximum effort into the task most of the time, the users would only seldom take initiative and hence fail to gain training experience.

On the other hand, in many applications, users would prefer comfort over having a better sense of interaction. For instance, when working with an assistive robot in a cooperative manipulation task, users would prefer to finish the task in the fastest and the least tiring way. In such a setting, WPRA would be the better alternative as it optimizes for task performance and human effort. Finally, in some settings such as physical interaction with the elderly or the children, subjective sense of comfort, pleasure, and trust could matter the most, making CRA a better choice.

9 Conclusion

In this paper we present a systematic analysis of cooperative human-robot manipulation and introduce three different schemes for the allocation of effort resulting from the task. The envisaged cooperative load transport task is decomposed into the subtasks of steering and progressing according to the objects geometrical and dynamical properties. Meaningful decompositions are derived in order to parameterize policies to distribute the effort among the contributing partners. The effort along the direction of redundant inputs is allocated among the agents in terms of roles following three proposed strategies. The experimental evaluation revealed the interesting effect that a continuous dynamic role allocation policy is objectively superior over a constant role strategy whereas the human partners subjectively preferred the constant role which was more obvious.

Our next steps include the application of our dynamic role allocation scheme to more complex tasks involving dynamically changing environments with a stronger emphasis on different capabilities of the partners. Furthermore, possibilities to generate the underlying reference object trajectory will be investigated in more detail. We are convinced that the ability of a robotic system to adjust its own role within a cooperation is a relevant factor for the usefulness of future physical robotic assistants. The decrease of subjective acceptance of a dynamically changing role in spite of the performance increase leaves a number of interesting research questions.

Funding

This work is supported in part within the DFG excellence initiative research cluster "Cognition for Technical Systems – CoTeSys": `www.cotesys.org`.

A Index to Multimedia Extensions

Extension	Type	Description
1	Video	Sample trial as performed in the user study

References

D. Abbink, M. Mulder, and E. Boer. Haptic shared control: smoothly shifting control authority? *Cogn., Technol. & Work*, 14:19–28, 2012.

D. Althoff, O. Kourakos, M. Lawitzky, A. Mörtl, M. Rambow, F. Rohrmüller, D. Brscic, D. Wollherr, S. Hirche, and M. Buss. An Architecture for Real-time Control in Multi-robot Systems. In *Cognitive Systems Monographs*, pages 43–52. Springer, 2009.

C. Atkeson, C. An, and J. Hollerbach. Estimation of Inertial Parameters of Manipulator Loads and Links. *Int. J. Rob. Res.*, 5(3):101–119, 1986.

C. Basdogan, C.-H. Ho, M. Srinivasan, and M. Slater. An Experimental Study on the Role of Touch in Shared Virtual Environments. *ACM Trans. Comput.-Hum. Interact.*, 7(4):443–460, 2000. ISSN 1073-0516.

B. Donald, P. Xavier, J. Canny, and J. Reif. Kinodynamic Motion Planning. *J. Assoc. Comput. Mach.*, 40(5):1048–1066, 1993.

K. Doty, C. Melchiorri, and C. Bonivento. A Theory of Generalized Inverses Applied to Robotics. *Int. J. Robot. Res.*, 12:1–19, 1993.

P. Evrard and A. Kheddar. Homotopy Switching Model for Dyad Haptic Interaction in Physical Collaborative Tasks. In *Proc. EHS EuroHaptics*, pages 45–50, 2009.

D. Feth, R. Groten, A. Peer, S. Hirche, and M. Buss. Performance Related Energy Exchange in Haptic Human-Human Interaction in a Shared Virtual Object Manipulation Task. In *Proc. EHS EuroHaptics'09*, pages 338–343, 2009.

T. Flash and N. Hogan. The coordination of arm movements: An experimentally confirmed mathematical model. *J. Neurosci.*, 5:1688–1703, 1985.

B.A.C. Forsyth and K.E. Maclean. Predictive haptic guidance: intelligent user assistance for the control of dynamic tasks. *IEEE Trans. Vis. Comp. Graph.*, 12(1):103 –113, 2006.

D.W. Franklin, R. Osu, E. Burdet, M. Kawato, and T.E. Milner. Adaptation to stable and unstable dynamics achieved by combined impedance control and inverse dynamics model. *J. Neurophys.*, 90(5): 3270–3282, 2003.

R. Gillespie, J. Colgate, and M. Peshkin. A General Framework for Cobot Control. *IEEE Trans. Robot. Automat.*, 17(4):391–401, 2001.

R. Groten, D. Feth, H. Goshy, A. Peer, D.A. Kenny, and M. Buss. Experimental Analysis of Dominance in Haptic Collaboration. In *Proc. IEEE Ro-Man*, pages 723–729, 2009.

U. Hanebeck, N. Saldic, and G. Schmidt. A Modular Wheel System for Mobile Robot Applications. In *Proc. IEEE/RSJ IROS*, pages 17–22, 1999.

S. G. Hart and L. E. Stavenland. Development of NASA-TLX (Task Load Index): Results of empirical and theoretical research. In P. A. Hancock and N. Meshkati, editors, *Human Mental Workload*, chapter 7, pages 139–183. Elsevier, 1988.

Y. Hirata and K. Kosuge. Distributed Robot Helpers Handling a Single Object in Cooperation with Human. In *Proc. IEEE ICRA*, pages 458–463, 2000.

R. Ikeura, H. Monden, and H. Inooka. Cooperative motion control of a robot and a human. In *Proc. IEEE RO-MAN*, pages 112 –117, 1994.

R. Ikeura, T. Moriguchi, and K. Mizutani. Optimal variable impedance control for a robot and its application to lifting an object with a human. In *Proc. IEEE RO-MAN*, pages 500 – 505, 2002.

A. Kheddar. Human-robot haptic joint actions Is an equal control-sharing approach possible? In *Proc. IEEE HSI*, pages 268–273, 2011.

A. Kirsch, T. Kruse, E. Sisbot, R. Alami, M. Lawitzky, D. Brščić, S. Hirche, P. Basili, and S. Glasauer. Plan-Based Control of Joint Human-Robot Activities. *Künstl. Intell.*, 24(3):223–231, 2010.

K. Kosuge and Y. Hirata. Human-Robot Interaction. In *Proc. IEEE ROBIO*, pages 8–11, 2004.

K. Kosuge, H. Yoshida, and T. Fukuda. Dynamic control for robot-human collaboration. In *Proc. IEEE Intl. Workshop on Robot and Human Communication*, pages 398–401, 1993.

A. Kucukyilmaz, M. Sezgin, and C. Basdogan. Conveying Intentions through Haptics in Human-Computer Collaboration. In *Proc. IEEE WHC*, pages 421–426, June 2011.

M. Lawitzky, A. Mörtl, and S. Hirche. Load Sharing in Human-Robot Cooperative Manipulation. In *Proc. IEEE Ro-Man*, pages 185–191, 2010.

Y. Maeda, T. Hara, and T. Arai. Human-Robot Cooperative Manipulation without Motion Estimation. In *Proc. IEEE/RSJ IROS*, pages 2240–2245, 2001.

J.R. Medina, M. Lawitzky, A. Mörtl, D. Lee, and S. Hirche. An Experience-Driven Robotic Assistant Acquiring Human Knowledge to Improve Haptic Cooperation. In *Proc. IEEE IROS*, 2011.

S. Miossec and A. Kheddar. Human motion in cooperative tasks: Moving object case study. In *Proc. IEEE ROBIO*, pages 1509–1514, 2008.

R.M. Murray, Z. Li, and S.S. Sastry. *A mathematical introduction to robotic manipulation*, chapter Multifingered Hand Kinematics. CRC Press, 1994.

N. Nitzsche, U. Hanebeck, and G. Schmidt. Design Issues of Mobile Haptic Interfaces. *J. Robot. Syst.*, 20(9):549–556, 2003.

O. Oguz, A. Kucukyilmaz, T. Sezgin, and C. Basdogan. Haptic Negotiation and Role Exchange for Collaboration in Virtual Environments. In *Proc. IEEE HAPTICS'10*, pages 371–378, 2010.

R. Olfati-Saber, A. Fax, and R. Murray. Consensus and Cooperation in Networked Multi-Agent Systems. *Proc. IEEE*, 95:215–233, 2007.

C.A.C. Parker and E.A. Croft. Experimental investigation of human-robot cooperative carrying. In *Proc. IEEE/RSJ IROS*, pages 3361 –3366, 2011.

L. Parker. Distributed Intelligence: Overview of the Field and its Application in Multi-Robot Systems. *J. Phys. Agents*, 2:5–14, 2008.

C. Passenberg, R. Groten, A. Peer, and M. Buss. Towards real-time haptic assistance adaptation optimizing task performance and human effort. In *Proc. IEEE WHC*, pages 155 –160, 2011.

D. Prattichizzo and J. Trinkle. Grasping. In B. Siciliano and O. Khatib, editors, *Springer Handbook of Robotics*. Springer, Berlin, Heidelberg, 2008.

K. Reed and M. Peshkin. Physical Collaboration of Human-Human and Human-Robot Teams. *IEEE Trans. Haptics*, 1(2):108–120, 2008.

K. Reed, M. Peshkin, M. Hartmann, E. Colgate, and J. Patton. Kinesthetic Interaction. In *Proc. IEEE ICORR*, pages 569–574, 2005.

K. Reed, M. Peshkin, M. Hartmann, J. Patton, P. Vishton, and M. Grabowecky. Haptic cooperation between people, and between people and machines. In *Proc. IEEE/RSJ IROS*, pages 2109–2114, 2006.

L.B. Rosenberg. Virtual fixtures: Perceptual tools for telerobotic manipulation. In *Proc. IEEE Virtual Reality Annual International Symposium*, pages 76 –82, 1993.

A.F. Salleh, R. Ikeura, S. Hayakawa, and H. Sawai. Cooperative Object Transfer: Effect of Observing Different Part of the Object on the Cooperative Task Smoothness. *J. Biomech. Sci. Eng.*, 6(4):343–360, 2011.

S. Schneider and R. Cannon. Object Impedance Control for Cooperative Manipulation: Theory and Experimental Results. *IEEE Trans. Robot. Automat.*, 8(3):383–394, 1992.

B. Stanczyk and M. Buss. Development of a Telerobotic System for Exploration of Hazardous Environments. In *Proc. IEEE/RSJ IROS*, pages 2532–2537, 2004.

T. Takubo, H. Arai, Y. Hayashibara, and K. Tanie. Human-Robot Cooperative Manipulation Using a Virtual Nonholonomic Constraint. *Int. J. Robot. Res.*, 21:541–553, 2002.

A. Thobbi, Y. Gu, and W. Sheng. Using Human Motion Estimation for Human-Robot Cooperative Manipulation . In *Proc. IEEE/RSJ IROS*, pages 2873–2878, 2011.

U. Unterhinninghofen, T. Schauß, and M. Buss. Control of a Mobile Haptic Interface. In *Proc. IEEE ICRA*, pages 2085–2090, 2008.

T. Wojtara, M. Uchihara, H. Murayama, S. Shimoda, S. Sakai, H. Fujimoto, and H. Kimura. Human-robot collaboration in precise positioning of a three-dimensional object. *Automatica*, 45(2): 333 – 342, 2009.